

A CRS oedometer cell for unsaturated and non-isothermal tests

Bagheri, M., Mousavi Nezhad, M. & Rezania, M.

Author post-print (accepted) deposited by Coventry University's Repository

Original citation & hyperlink:

Bagheri, M, Mousavi Nezhad, M & Rezania, M 2019, 'A CRS oedometer cell for unsaturated and non-isothermal tests' *Geotechnical Testing Journal*, vol. 43, no. 1, GTJ20180204.

<https://dx.doi.org/10.1520/GTJ20180204>

DOI 10.1520/GTJ20180204

ISSN 0149-6115

Publisher: ASTM International

Copyright © and Moral Rights are retained by the author(s) and/ or other copyright owners. A copy can be downloaded for personal non-commercial research or study, without prior permission or charge. This item cannot be reproduced or quoted extensively from without first obtaining permission in writing from the copyright holder(s). The content must not be changed in any way or sold commercially in any format or medium without the formal permission of the copyright holders.

This document is the author's post-print version, incorporating any revisions agreed during the peer-review process. Some differences between the published version and this version may remain and you are advised to consult the published version if you wish to cite from it.



A CRS Oedometer Cell for Unsaturated and Non-Isothermal Tests

Journal:	<i>Geotechnical Testing Journal</i>
Manuscript ID	GTJ-2018-0204.R3
Manuscript Type:	Technical Manuscript
Date Submitted by the Author:	n/a
Complete List of Authors:	Bagheri, Meghdad; University of Nottingham Mousavi Nezhad, Mohaddeseh ; University of Warwick Rezania, Mohammad; University of Warwick,
ASTM Committees and Subcommittees:	D18.05 Strength and Compressibility of Soils < D18 Committee on Soil and Rock
Keywords:	oedometer, strain rate, temperature, suction, tensiometer, water retention, calibration, compression tests
Abstract:	<p>Research into the thermo-hydro-mechanical (THM) behavior of unsaturated soils and the effect of strain rate on their mechanical responses requires employment of advanced laboratory testing systems and procedures as well as protocols of correcting the measured data in order to account for errors associated with complex test conditions and apparatus calibrations. This paper presents design and calibration of an innovative constant-rate-of-strain (CRS) oedometer cell for characterization of the THM behavior of soils under combined non-isothermal and unsaturated conditions. The advanced oedometer cell enables for simultaneous control of temperature, suction, and stress state within the soil specimens. Temperatures of 20 to 200° C is applied through a tubular heating element placed at the base of the soil specimen. Suction is controlled using axis-translation technique, and measured using both axis-translation and two high-capacity tensiometers (HCTs) accommodated on the periphery of the specimen. The performance of the new cell is assessed based on a set of tests performed on clay specimens and its merits and advantages are discussed in detail.</p>

SCHOLARONE™
Manuscripts

A CRS Oedometer Cell for Unsaturated and Non-Isothermal Tests

Meghdad Bagheri¹, Mohaddeseh Mousavi Nezhad², Mohammad Rezania³

¹Department of Civil Engineering, University of Nottingham, Nottingham, UK

^{2,3}School of Engineering, University of Warwick, Coventry, UK

Abstract

Research into the thermo-hydro-mechanical (THM) behavior of unsaturated soils and the effect of strain rate on their mechanical responses requires employment of advanced laboratory testing systems and procedures as well as protocols of correcting the measured data in order to account for errors associated with complex test conditions and apparatus calibrations. This paper presents design and calibration of an innovative constant-rate-of-strain (CRS) oedometer cell for characterization of the THM behavior of soils under combined non-isothermal and unsaturated conditions. The advanced oedometer cell enables for simultaneous control of temperature, suction, and stress state within the soil specimens. Temperatures of 20 to 200° C is applied through a tubular heating element placed at the base of the soil specimen. Suction is controlled using axis-translation technique, and measured using both axis-translation and two high-capacity tensiometers (HCTs) accommodated on the periphery of the specimen. The

¹ Email: meghdad.bagheri@nottingham.ac.uk

² Email: m.mousavi-nezhad@warwick.ac.uk

³ Corresponding author, Email: m.rezania@warwick.ac.uk

19 performance of the new cell is assessed based on a set of tests performed on clay specimens
 20 and its merits and advantages are discussed in detail.

21 **Keywords:** oedometer, strain rate, temperature, suction, tensiometer, water retention,
 22 calibration, compression tests.

23 **List of Symbols**

$\dot{\varepsilon}_v$ = volumetric strain rate
 ΔL_T = thermally induced axial deformation
 ΔT = temperature change
 Δu = pore-water pressure change
 ε_a = axial strain
 σ_p = yield vertical net stress
 σ_v = applied vertical total stress
 c_v = coefficient of consolidation
 G_s = specific gravity
 I_p = plasticity index
 s = soil suction
 s_0 = initial suction
 S_r = degree of saturation
 T = temperature
 u_a = pore-air pressure
 u_{exc} = excess pore-water pressure
 u_w = pore-water pressure
 w = gravimetric water content
 w_0 = initial gravimetric water content
 w_L = liquid limit
 w_P = plastic limit
 AEV = air-entry value
 CG = constant gradient
 CL = continuous loading
 CRL = constant rate of loading
 CRS = constant rate of strain
 D = grain size
 HCT = high capacity tensiometer
 IL = incremental loading
 LC = London clay
 LPT = linear potentiometric transducer
 PSD = particle size distribution
 PWPT = pore-water pressure transducer

1
2
3 SWRC = soil water retention curve

4 TC = thermocouple

5
6 THM = thermo-hydro-mechanical
7
8

9 24 Introduction

10
11 25 Climate interacts with natural slopes and shallow depth soil deposits to cause changes in their
12
13 26 hydro-mechanical properties mainly in terms of their pore-water pressure (u_w), strength and
14
15 27 stiffness parameters (Delage et al. 2000; Burghignoli et al. 2000; Cekerevac and Laloui 2004).

16
17
18 28 These deposits are typically encountered above the phreatic table and hence, are unsaturated.

19
20
21 29 Under these conditions, different physical processes with high level of coupling take place.

22
23 30 These processes mainly involve; (1) hydraulic processes such as liquid and/or vapor flow,
24
25 31 stemming from groundwater recharge, precipitation, evaporation, and evapotranspiration (e.g.

26
27
28 32 Ng and Xu 2012; Pagano et al. 2016), (2) thermal processes such as natural or artificial heat

29
30
31 33 transfer induced by droughts, hot buried pipes and cables, and underground thermal energy

32
33 34 storage systems (e.g. Salager et al. 2008; Uchaipichat and Khalili 2009), and (3) mechanical

34
35 35 processes such as solid matrix deformations induced by sedimentation, progressive

36
37 36 gravitational straining, and/or external loading (e.g. Lai et al. 2010; Zou et al. 2013). Moreover,

38
39 37 it is well known that the mechanical behavior of soils, in particular natural soft soils, is highly

40
41
42 38 influenced by time and rate effects (Bagheri et al. 2015; Rezanian et al. 2016; Rezanian et al.

43
44 39 2017). Experimental investigation and numerical modelling of soils behavior subjected to each

45
46 40 of these processes are relatively complex and costly. The coupling of these processes can

47
48 41 indeed further complicate the investigations, requiring advanced numerical modelling tools and

49
50 42 laboratory and field testing equipment. The difficulty in control of several parameters in an

51
52 43 experiment and to ensure their accurate measurement might be a reason for limited number of

53
54 44 experimental studies on coupled effects of stress state, suction, and temperature (François and

55
56 45 Laloui 2010). In all abovementioned processes, characterization of soils' one-dimensional (1D)

57
58 46 stress-strain response is of high importance especially for serviceability and stability analysis
59
60

1
2
3 47 of geotechnical structures. In the past few decades, researchers have been working on development of
4
5 48 1D testing equipment which allow for testing soils under controlled stress, strain, suction, and
6
7 49 temperature conditions. Several apparatuses have been so far devised and constructed. A
8
9 50 suction and temperature controlled oedometer cell was developed by [Romero et al. \(1995\)](#) at
10
11 51 the Technical University of Catalonia (UPC), Spain. In this apparatus, axial stress is imposed
12
13 52 through an air-pressurized stretchable diaphragm. Temperature is applied and regulated using
14
15 53 a thermostatically controlled heater surrounding the cell, and suction is controlled using axis-
16
17 54 translation technique which is based on measurement of air and water pressure differential
18
19 55 across a high air-entry value (AEV) ceramic disk. A number of limitations associated with axis-
20
21 56 translation method have been reported in the literature including; (1) the range of suctions that
22
23 57 can be measured or applied is a function of the AEV of the ceramic filter as well as the
24
25 58 maximum capacity of the pressurized air supply system, (2) lack of good contact between the
26
27 59 pore-water and the water in the ceramic disk results in discontinuity of water flow through the
28
29 60 porous filter and may dramatically increase the equilibrium time or even prohibit the drainage
30
31 61 of water ([Marinho et al. 2008](#)), (3) accumulation of diffused air bubbles in high AEV ceramic
32
33 62 can result in discontinuity between the specimen's pore-water and the water in the
34
35 63 measurement system ([Romero et al. 2003](#)), (4) control of soil moisture evaporation can be
36
37 64 rather difficult, requiring a careful setup of auxiliary devices such as vapor traps and diffused
38
39 65 air flushing/volume indicator, especially when testing at high temperatures ([Romero et al.](#)
40
41 66 [2003](#); [Romero et al. 2005](#)). [Rampino et al. \(1999\)](#) developed a suction controlled oedometer
42
43 67 cell for unsaturated soils at Università di Napoli Federico II, Italy. Their design was based on
44
45 68 the modifications applied to the device initially designed by [Wissa and Heiberg \(1969\)](#). This
46
47 69 apparatus allows for running all types of continuous loading (CL) tests, i.e. CRS, constant rate
48
49 70 of loading (CRL), and constant gradient (CG) tests. Axial stress in this system is applied
50
51 71 directly through an air pressurized chamber connected to the loading cap of the cell. This
52
53
54
55
56
57
58
59
60

1
2
3 72 device, similar to the UPC oedometer, controls matric suction of the specimen using the axis-
4
5 73 translation technique and, therefore, is prone to the drawbacks associated with this method.
6
7
8 74 [Tarantino and De Col \(2008\)](#) performed static compaction tests on Kaolin Clay specimens
9
10 75 inside an oedometer cell modified to measure suction variations using two HCTs
11
12 76 accommodated on its loading cap. In this apparatus, the axial stress is applied to the sample
13
14
15 77 using a pneumatic actuator, hence allowing for CRS tests to be carried out. CRS test results on
16
17 78 undisturbed unsaturated Bapaume loess specimens using a modified oedometer cell were
18
19 79 reported by [Muñoz-Castelblanco et al. \(2011\)](#). The oedometer cell is equipped with a HCT
20
21 80 accommodated at the base of the specimen for direct measurement of soil suction evolutions
22
23 81 during constant water content CRS tests carried out at rates of 0.003, 0.010, and 0.059 %min⁻¹.
24
25 82 ¹. [Tarantino and De Col \(2008\)](#) and [Muñoz-Castelblanco et al. \(2011\)](#) concluded that CRS tests
26
27 83 are preferred over the conventional incremental loading (IL) tests for monitoring suction
28
29 84 variations and that the IL tests are better adapted for saturated specimens. Design of a suction
30
31 85 and temperature controlled oedometer cell at the Ecole Polytechnique Fédérale de Lausanne
32
33 86 (EPFL), Switzerland, was also reported by [François and Laloui \(2010\)](#). In this device, the axial
34
35 87 stress is applied through a water pressurized membrane made of a stretchable material. Heating
36
37 88 is applied through circulating heated water in a ring-shaped chamber surrounding the specimen.
38
39
40 89 Axis-translation is used as the suction control method. The drawbacks of this apparatus,
41
42 90 however, can be outlined as; (1) use of stretchable membranes to transmit the vertical pressure
43
44 91 to the specimen typically involves difficulties in calibration of membrane friction with the cell
45
46 92 wall, (2) errors associated with membrane fatigue influences and modifies the mechanical
47
48 93 loading transmitted to the specimen in long term use, and (3) the drawbacks of axis-translation
49
50 94 technique, as explained above, can further influence the test results. A temperature controlled
51
52 95 CRS oedometer cell was developed by [Tsutsumi and Tanaka \(2011\)](#) at Hokkaido University,
53
54 96 Japan. A high accuracy stepper motor system is utilized in this apparatus for loading the
55
56
57
58
59
60

1
2
3 97 specimen under very small strain rates. An external load cell placed at the bottom of the cell is
4
5 98 used to measure the axial stresses. The specimen's temperature is controlled through circulation
6
7 99 of an isothermal liquid inside a metal pipe spiraled around the specimen. A thermocouple
8
9 100 attached to the upper platen of the consolidation cell is used for measurement of temperature
10
11 101 variations. The main drawback of this device is the use of external load cell which involves
12
13 102 errors associated with the friction between the loading ram and the guide shaft. [Coccia and](#)
14
15 103 [McCartney \(2016\)](#) studied the thermal volume change of unsaturated compacted Bonny silt in
16
17 104 a high pressure thermal isotropic cell equipped with pressure-volume controllers to track
18
19 105 changes in degree of saturation. In this cell, matric suction is controlled via the axis translation
20
21 106 technique. The thermal volume change behavior of soils with different stress histories was
22
23 107 found to be significantly influenced by the secondary compression response. Most recently, a
24
25 108 temperature controlled CRS oedometer cell was developed by [Jarad et al. \(2017\)](#) at Université
26
27 109 de Lorraine, France. This cell is installed in a load frame capable of running strain-controlled
28
29 110 tests in range of $0.002 - 0.02 \text{ \%min}^{-1}$. A temperature range of 5 to 70° C could be applied to
30
31 111 the specimen through circulation of a thermal liquid in a spiral tube positioned around the cell
32
33 112 (similar to the cell developed at Hokkaido University). The cell chamber is filled with water to
34
35 113 ensure fully saturated conditions throughout the experiments. [Ng et al. \(2017\)](#) developed a
36
37 114 thermal oedometer with invar ring and studied the effect of boundary conditions on cyclic
38
39 115 thermal strains of clay and sand samples. In this cell, cyclic heating and cooling is applied
40
41 116 through heat exchange with the heated water circulated through a spiral tube placed around the
42
43 117 soil specimen.

44
45 118 The advanced apparatuses discussed above generally suffer from technical design drawbacks
46
47 119 that restrict their application for long-term tests and over a wide range of soil suction and
48
49 120 temperatures. For example, using axis-translation method to control matric suction in a
50
51 121 specimen subjected to a long-term 1D creep or stress relaxation test can cause excessive

1
2
3 122 evaporation of soil water as well as air diffusion through the ceramic disk and hence, errors in
4
5 123 monitoring suction and volume change evolutions. This paper presents the design and
6
7 124 calibration of a new oedometer cell for conducting strain controlled compression tests while
8
9 125 controlling and measuring suction and temperature of the specimen. Incorporation of two
10
11 126 suction control and measurement methods, i.e. axis-translation and HCT, allows for successful
12
13 127 monitoring of soil matric suction during short-term and long-term consolidation and stress
14
15 128 relaxation tests with minimal errors. Conducting 1D compression tests under controlled strain
16
17 129 rate, suction, and temperature requires rigorous calibrations and experimental techniques. The
18
19 130 experimental procedures for correcting the applied conditions and measured data during
20
21 131 experiments are discussed in details and some preliminary test results highlighting the coupled
22
23 132 effects of strain rate ($\dot{\epsilon}_v$), soil suction (s), and temperature (T) on compressibility of clay
24
25 133 samples are presented.
26
27
28
29
30
31

32 134 The New CRS Oedometer

33 135 *CELL LAYOUT*

34
35 136 Fig. 1 shows a schematic diagram of the cell structure. The outer cell body is made of AISI 304
36
37 137 stainless steel whereas the inner cell and the confining ring are made of brass. The cell wall is
38
39 138 designed to be thick enough to support the specimen and prevent lateral deformation, and hence
40
41 139 satisfy the k_0 conditions. To minimize the disturbance to the specimen, the loading cap is made
42
43 140 of a lightweight material i.e. aluminium. Cylindrical soil specimens of 95 mm diameter and 35
44
45 141 mm height can be tested in this apparatus. These dimensions are compatible with the minimum
46
47 142 specimen diameter to thickness ratio of 2.5 recommended by ASTM standard for consolidation
48
49 143 testing ([ASTM-D4186-06 2006](#)). Generally, the in-situ settlement rates of full-scale structures
50
51 144 are much greater than those obtained from conventional oedometer tests on small size
52
53 145 specimens (e.g. 75 mm diameter \times 20 mm thickness). This can be attributed to the effect of
54
55
56
57
58
59
60

1
2
3 146 the clay macrofabric on drainage behavior (Rowe and Barden 1966). In fact, the
4
5 147 macrostructural properties of clay layers such as presence of thin layers of silt and sand, organic
6
7 148 inclusions, and silt-filled fissures can increase the overall permeability of the clay deposit and
8
9 149 hence, increase settlement rates (Craig 2004). Garga (1988) performed oedometer tests on
10
11 150 fissured London Clay (LC) specimens of various diameters and reported that the coefficient of
12
13 151 consolidation (c_v) from 100 mm diameter specimens were approximately 50% higher than 76
14
15 152 mm diameter specimens. More recently, Gasparre (2005) reported that the existence of fissures
16
17 153 in 100 mm diameter specimens of intact LC can be the most possible reason for the observed
18
19 154 differences in shear strength of 100 mm and 38 mm diameter specimens in triaxial tests.
20
21 155 Therefore, in order to obtain more realistic predictions of soil settlements in laboratory, it is
22
23 156 necessary to perform experiments on specimens large enough to represent structural
24
25 157 (macrofabric) features of natural clays. In the new CRS cell, an increase in the diameter and
26
27 158 the height of the specimen by respectively 27% and 75%, resulted in an increase in the
28
29 159 specimen's volume by 181%, increasing the possibility of capturing macrostructural effects on
30
31 160 hydro-mechanical properties. Furthermore, the selected dimensions allows for coring
32
33 161 undisturbed specimens from U100 tube samplers with minimum disturbance.
34
35
36
37
38
39
40

41 162 *STRESS/STRAIN CONTROL AND MEASUREMENT*

42
43 163 The apparatus is a load frame based system (Fig. 2) where the loading is generally via feedback
44
45 164 from a velocity controlled load frame. The loading frame has a maximum compressive strength
46
47 165 of 50 kN and speed range of 10^{-5} – 10 mm/min for constant rate of displacement. A 25 mm
48
49 166 travel length linear potentiometric transducer (LPT) placed on the top platen of the cell
50
51 167 provides measurement of axial strain and, therefore, volume change of the specimen. Axial
52
53 168 force is measured by an internal 25 kN submersible load cell guided through a ball bearing
54
55 169 shaft on the top platen of the cell. The use of internal load cells rectifies the adverse effect of
56
57 170 friction on measurements typical of conventional external load cells. This improvement is
58
59
60

1
2
3 171 highlighted during creep and stress relaxation tests (Fodil et al. 1997). The load cell is screwed
4
5 172 to the loading cap and, from the other end, to the load frame to allow for strain controlled
6
7
8 173 unloading of the specimen.
9

11 174 *MATRIC SUCTION CONTROL AND MEASUREMENT*

13
14 175 The specific design of the CRS oedometer cell enables performance of strain controlled
15
16 176 consolidation tests under both saturated (pore-water pressure control) and unsaturated (suction
17
18 177 control) conditions. A 1.5 MPa high AEV porous disk placed at the bottom of the specimen
19
20 178 allows for testing soil specimens under suction controlled conditions. Matric suctions of up to
21
22
23 179 1.0 MPa can be imposed using axis-translation technique. Pore-air pressure (u_a), supplied from
24
25 180 a high-pressure air compressor and regulated by a pressure panel, is applied to the top of the
26
27 181 specimen. The porous stone at the top of the specimen helps for uniform distribution of air
28
29 182 pressure across the sample area. Pore-water pressure (u_w) is controlled at the bottom of the
30
31
32 183 specimen and regulated by an air-water interface (bladder) and a pressure panel. Using axis-
33
34 184 translation technique for applying suction to the specimen typically involves evaporation of
35
36 185 soil water, and the generation of vapor fluxes causes unwanted variation of suction inside the
37
38 186 specimen. This effect is further highlighted when testing unsaturated specimens under high
39
40 187 temperatures. To restrict the vapor transfer, as suggested by François and Laloui (2010), a
41
42 188 vapor trap was installed in the air pressure line to humidify the pressurized air and maintain a
43
44 189 high order of relative humidity throughout the experiments. Moreover, as recommended by
45
46 190 Romero et al. (2005), to control the air diffusion across the high AEV ceramic disk, a flushing
47
48 191 system was incorporated at the base of the cell, to periodically flush the diffused air bubbles.
49
50
51 192 The spiral circuit machined inside the pedestal and underneath the porous disk further helps in
52
53 193 collection of the diffused air bubbles from the system (Rampino et al. 1999). A 3.5 MPa pore-
54
55 194 water pressure transducer (PWPT) is used for measurement of positive u_w at the base of the
56
57
58 195 specimen. Water volume exchanges are measured using a semi-automatic volume change
59
60

1
2
3 196 apparatus looped with the bladder and the pressure panel. Furthermore, two in-house made
4
5 197 HCTs (see Bagheri et al. 2018) accommodated over the periphery and at the mid height of the
6
7
8 198 specimen provide continuous measurement of matric suction during the experiments.
9
10 199 Accommodating HCTs over the periphery and at the mid-height of the specimen allows for
11
12 200 measurement of an average u_w during the tests. HCTs can be also used for local measurement
13
14 201 of positive u_w inside the specimen. The specific assembly of the tensiometers inserts enables
15
16
17 202 for replacement of cavitated tensiometers during the experiments without any interruption to
18
19 203 the tests and disturbing the specimen.
20
21
22

23 204 *TEMPERATURE CONTROL SYSTEM*

25 205 The heating system consists of a WATROD double-ended tubular heater element (supplied by
26
27 206 Watlow Ltd), placed at the base of the cell, and two J-type thermocouples for measurement and
28
29 207 monitoring of temperature variations on the cell's body and inside the specimen. A temperature
30
31 208 control unit is used for setting target temperatures and monitoring feedbacks from the
32
33 209 thermocouples. Temperature variations inside the specimen are measured by a thermocouple
34
35 210 (TC1) placed close to the specimen. Another thermocouple (TC2) located close to the heater
36
37 211 records the cell temperature. The signal feedback from this thermocouple is used to keep the
38
39 212 temperature constant by acting on the thermostat in the control unit. The heating system enables
40
41 213 testing soil specimens over a temperature range of 20 to 200° C. The average heating/cooling
42
43 214 rate is approximately 3° C per minute on automatic mode. This rate can also be manually
44
45 215 controlled by setting target temperatures at pre-defined time intervals. For example, a
46
47 216 temperature change of 30° C could be ramped up over 30 minutes if the unit is set to increase
48
49 217 the temperature for 1° C at every minute. An isolating ring made of Tufnol material is placed
50
51 218 between the cell base and the loading piston's platen to prevent any possible damages to the
52
53 219 stepper motor as a result of heat transfer.
54
55
56
57
58
59
60

220 *DATA ACQUISITION*

221 An 8 channel serial pad (GEODATALOG8 supplied from Controls Testing Equipment) was
222 used for data acquisition from the transducers (load cell, LPT, and PWPT). The built-in data
223 acquisition software enables for offline monitoring and storage of the data. The HCTs
224 measurements were also monitored using a National Instruments (NI) data acquisition system
225 and LabVIEW software. A LabVIEW code was also developed for monitoring the feedback
226 data from the thermocouples. All the feedback data from the transducers and the temperature
227 control unit were continually stored on a computer.

228 *Calibration Procedures*

229 As for any laboratory testing systems, a rigorous calibration was necessary in order to account
230 for the errors associated with temperature change and mechanical adjustments during
231 experiments. To this end, an assessment of (i) the effect of friction between the loading cap's
232 O-ring and the internal wall of the cell, (ii) the expansion and contraction of the cell under
233 temperature changes, (iii) the effect of temperature on HCTs, and (iv) the thermal equilibrium
234 between the heating system and the specimen were carried out and necessary calibrations were
235 applied. In the following subsections, the results of these calibrations are presented.

236 *INNER WALL FRICTION*

237 Friction between the loading cap's O-rings and the internal wall of the cell as well as between
238 the sample and the inner wall of the cutting ring, are the main sources of possible sidewall
239 friction. In order to minimize the effect of sidewall friction on the measured forces several
240 methodologies can be considered. Lubricating the O-rings on the loading cap as well as the
241 internal cell body and the inner periphery of the cutting ring, with a very thin layer of grease,
242 can to some extent reduce the sidewall friction (Seah and Juimarongrit 2003). Attention must
243 be applied not to leave high amount of grease on the cutting ring's inner wall, as grease can

1
2
3 244 influence the inter-particles friction within the soil specimen and modify the consolidation
4
5 245 process. [François and Laloui \(2010\)](#) performed a set of mechanical loading and unloading on
6
7 246 water placed in the sample chamber in order to quantify the effect of friction between the
8
9 247 loading membrane and the cell wall. A linear relationship was observed between the applied
10
11 248 and measured pressures showing 5 – 6% difference. [Sample-Lord and Shakelford \(2012\)](#)
12
13 249 performed a set of CRS consolidation tests on soil slurries containing bentonite and granular
14
15 250 zero valent iron in acrylic columns and reported that the increase in strain rate will increase the
16
17 251 induced friction between the top platen O-rings and the inner walls of the test cells. In this
18
19 252 study, the inner wall of the internal cell was polished to produce a very smooth and glossy
20
21 253 surface. Moreover, the loading cap's O-rings, the inner cell wall and the inner wall of the
22
23 254 cutting ring were lubricated with a very thin layer of Vaseline to further minimize any potential
24
25 255 side friction effect. Given the use of internal load cell in this work to allow for direct
26
27 256 measurement of the applied load at the contact point at the top of the specimen, calibration to
28
29 257 account for the side friction was not carried out in this study.
30
31
32
33
34
35

36 258 *CELL DEFORMATION UNDER CHANGES IN TEMPERATURE*

37
38
39 259 The deformability of the cell structure under temperature changes can be investigated in the
40
41 260 aspects of (i) the thermal expansion of the cell which can modify the measurements of the axial
42
43 261 strains, and (ii) the thermal expansion of the cutting ring which can alter the oedometric
44
45 262 conditions by posing undesirable radial deformations. Some researchers including [Romero et](#)
46
47 263 [al. \(2003\)](#) and [François and Laloui \(2010\)](#) investigated the thermal expansion effects on the
48
49 264 oedometric conditions and expressed that thermal strain of the soil particles partially offsets
50
51 265 the thermal expansion or contraction of the cutting ring and, therefore, the oedometric condition
52
53 266 is not significantly affected during non-isothermal experiments. Hence, it is only the thermal
54
55 267 effect on the axial strains that needs to be taken into account when correcting the obtained test
56
57 268 data. To this end, a simple calibration procedure was carried out. A cylindrical AISI 304
58
59
60

1
2
3 269 stainless steel sample with known coefficient of thermal expansion was placed inside the cell.
4
5 270 Afterwards, the cell was subjected to a heating and cooling cycle of 25 to 75° C in steps of 10°
6
7
8 271 C, and the corresponding axial deformation due to the thermal expansion of the sample and
9
10 272 metallic cell body was measured by the LPT. Having known the thermal dilation of the stainless
11
12 273 steel sample, the induced thermal dilation of the cell structure was deduced. Fig. 3 presents the
13
14 274 measured and corrected thermally induced deformation of the cell structure. The observed
15
16 275 differences in measured vertical displacements associated with heating and cooling cycles
17
18 276 might be due to the insufficient time given during cooling steps for thermal equilibrium and
19
20 277 recovery of thermally induced elastic strains. The axial deformation due to the effect of
21
22 278 temperature (ΔL_T) appears to vary linearly with applied temperature change (ΔT) and can be
23
24 279 approximated using the following linear correlation;

$$\Delta L_T = -0.0029\Delta T \quad (1)$$

31 280 The fact that the obtained values of ΔL_T are negative indicates that the thermal dilation of the
32
33 281 cell structure results in a compressive deformation. Basically, during compression, the axial
34
35 282 downward movement of the loading ram implies negative displacement measurement by the
36
37 283 attached LPT (its shaft moves upward). Similarly, thermal expansion of the cell and top platen
38
39 284 results in upward movement of the LPT's shaft, given that the loading ram is fixed to the load
40
41 285 frame. It must be mentioned that the thermal expansion of the frame is disregarded, as the
42
43 286 isolating ring made of Tufnol material, placed between the cell base and the loading piston's
44
45 287 platen, prevents any possible heat transfer to the load frame. Moreover, a temperature range of
46
47 288 20 to 80° C has been considered in most published works on the effect of temperature on THM
48
49 289 properties of clayey soils (e.g. [Delage et al. 2000](#); [Burghignoli et al. 2000](#); [Cekerevac and](#)
50
51 290 [Laloui 2004](#); [François and Laloui 2010](#); [Jarad et al. 2017](#)). Therefore, the same range was
52
53 291 considered in this work for calibrating the presented CRS cell and carrying out the preliminary
54
55 292 experiments. It must be mentioned here that same calibrations may not be extrapolated for
56
57
58
59
60

1
2
3 293 higher temperatures. Indeed, calibration and experimental investigations over the higher
4
5 294 temperatures ($>75^{\circ}\text{C}$) will be the subject of future studies using this apparatus.
6
7
8

9 295 *EFFECT OF TEMPERATURE ON HCT*

10
11 296 The HCTs were saturated and calibrated in an in-house made stainless steel saturation chamber
12
13 297 (Fig. 4) following the procedure described in Bagheri et al. (2018). The saturation chamber
14
15 298 possesses 8 slots to insert and clamp the HCTs in a way that their ceramic filter is faced inward
16
17 299 and prone to de-aired de-mineralized water. A screw piston positioned at the centre of the
18
19 300 chamber enables pressurization of the fluid inside the chamber. In order to evaluate the effect
20
21 301 of temperature on HCT calibrations, the HCTs were subjected to a loading and unloading cycle
22
23 302 inside the chamber, at two different temperatures of 25 and 60° C (Fig. 5). The obtained curves
24
25 303 exhibited a linear trend both for loading and unloading cycles. A linear extrapolation to the
26
27 304 calibration equation was developed for the pressures in negative range. An increase in
28
29 305 temperature resulted in an increase of voltage output and shift of the calibration curve, yet the
30
31 306 calibration coefficient was not affected notably. Considering the linear dilation of the HCT's
32
33 307 AISI 304 stainless steel body (see Fig. 3), it was assumed that the shift in voltage output with
34
35 308 temperature is also linear, resulting in an increase of the voltage output by 1 μV per 1° C
36
37 309 increase of temperature, corresponding to an increase in suction measurements by
38
39 310 approximately 10 kPa. Similar results were obtained for the other HCTs used. The data
40
41 311 obtained from HCTs during non-isothermal tests (see next section) were, therefore, adjusted
42
43 312 for the differences in calibration constants obtained during calibration of the HCTs at
44
45 313 corresponding temperatures.
46
47
48
49
50
51
52
53

54 314 *TEMPERATURE EQUILIBRIUM*

55
56 315 Due to the difference in thermal conductivity of the cell body and the soil specimen, a delay in
57
58 316 thermal equilibrium between the heating system and the soil specimen was expected. In order
59
60

1
2
3 317 to quantify this time lag, the cell was subjected to a thermal cycle of 25 to 65°C in steps of
4
5 318 10°C. Temperature variations during each step were recorded for approximately 50 minutes.
6
7
8 319 The thermal variations inside the saturated soil specimen was monitored using the
9
10 320 thermocouple TC1, while the thermal variations of the heating system was monitored using the
11
12 321 thermocouple TC2. It was observed that thermal equilibrium for each step of heating or cooling
13
14 322 was obtained in approximately 40 minutes (Fig. 6). The temperature control unit enables
15
16 323 applying a constant target temperature over the course of experiments, hence, maintaining
17
18 324 thermal equilibrium between the heating system and the soil specimen. At equilibrium, there
19
20 325 were not significant differences between the temperature in the heating system and the soil
21
22 326 specimen, indicating the efficiency of the isolating system. The significant reduction in the
23
24 327 equilibrium time in comparison with the similar temperature controlled systems presented in
25
26 328 the literature (e.g. [François and Laloui 2010](#)) is believed to be due to the heating from the base
27
28 329 of the specimen which rectifies, to some extent, the delays associated with thermal conductivity
29
30 330 of the metallic cell body. Moreover, direct heating of the cell's stainless steel base, using the
31
32 331 element heater, accelerates the thermal diffusion process in the metallic cell base. Therefore,
33
34 332 the thermal diffusion process in the soil mass may have more contribution to the observed
35
36 333 thermal equilibrium delay than the thermal diffusion in cell body.
37
38
39
40
41
42

43 334 Preliminary Tests

44 335 *MATERIAL AND SPECIMEN PREPARATION*

45
46 336 The material used for these tests was LC which was collected from an engineering site in Isle
47
48 337 of Sheppey, UK. To avoid complications associated with microfabric of undisturbed and
49
50 338 compacted soils, reconstituted samples were used for this set of experiments. The samples were
51
52 339 oven dried for 48 hours, then crushed into powder, and sieved through a 1.18 mm sieve.
53
54 340 Reconstituted soil samples were prepared by mixing the soil powder with distilled water at
55
56
57
58
59
60

1
2
3 341 initial water content of $w_0 = 1.5w_L$ until a homogenous paste was obtained. The paste was then
4
5 342 consolidated in a 120 mm diameter Perspex consolidometer under a vertical stress of 80 kPa
6
7 343 for a duration of 5 days. The sample was then quickly unloaded to avoid any swelling and water
8
9 344 absorption. The obtained cylindrical sample was then cut into three equal pieces and allowed
10
11 345 to dry at room temperature to pre-specified water contents. Each sub-sample was placed on a
12
13 346 course porous stone and inside a perforated chamber for relatively uniform water evaporation.
14
15 347 The porous stone was used to facilitate the dynamic drying process by exposing the specimen's
16
17 348 base to atmosphere. The unsaturated samples were then stored in air-tight containers for 24
18
19 349 hours for moisture equilibrium. Finally, the test specimens were prepared by carefully
20
21 350 penetrating the oedometer ring into the samples and trimming off the excess soil. It must be
22
23 351 noted that presence of course-grained peds (or large size clay clusters according to [Le et al.](#)
24
25 352 [2012](#)) resulted in an AEV value of around 250 kPa (see Fig. 8) which is notably lower than the
26
27 353 AEV of natural LC reported in the literature. The lower AEV made it possible to test specimens
28
29 354 over a wider range of suctions, lying on the desaturation phase of the soil water retention curve
30
31 355 (SWRC). Table 1 summarizes the index and physical properties of the reconstituted soil
32
33 356 samples.

34
35
36
37
38
39
40
41 357 Table 1. Index and physical properties of the reconstituted LC samples

Grain size, D (mm)			Index properties			
D < 0.002	0.002 < D < 0.063	D > 0.063	w_P	w_L	I_P	G_s
58%	30%	12%	18%	68%	50%	2.67

42
43
44
45
46
47
48
49 358 *EXPERIMENTAL PROCEDURE*

50
51
52 359 Before commencing each experiment, the preparation of the cell was carried out. The drainage
53
54 360 lines and the pressure transducer block were de-aired by means of vacuum and filled with de-
55
56 361 aired water. The lower and upper porous discs were also saturated. Functionality of all
57
58 362 transducers were checked and the load cell, LPT, and PWPT were zeroed. The specimen was
59
60

1
2
3 363 then placed inside the cell chamber. The two HCTs, which were preconditioned according to
4
5 364 the procedure described by [Bagheri et al. \(2018\)](#), were then installed on the periphery of the
6
7
8 365 specimen and gently clamped. Ultimate contact between the HCTs and the specimen was
9
10 366 ensured by applying soil paste to the HCTs' porous disks. The loading cap, with its lubricated
11
12 367 O-rings, was then positioned on top of the specimen and the load cell together with the top
13
14 368 platen were placed and fastened. The cell was set up on the load frame and an initial vertical
15
16 369 stress of 10 kPa was applied to the specimen to eliminate any possible bedding effects. The
17
18 370 HCTs were allowed to equilibrate for 2 – 3 hours. Axial load was applied to the specimen from
19
20 371 the piston moving upwards at constant rate of displacement, compressing the specimen inside
21
22 372 the confining ring. Drained CRS compression tests with continuous pore-water pressure
23
24 373 (suction) monitoring were carried out on reconstituted specimens at two different initial water
25
26 374 contents of 32 and 33%, and two different temperatures of 22 and 50° C. Two different strain
27
28 375 rates of 4.8×10^{-7} (denoted by letter A) and $2.4 \times 10^{-6} \text{ s}^{-1}$ (denoted by letter B) were selected
29
30 376 and used for this set of experiments. The values of strain rates were selected so as to be; (1)
31
32 377 compatible with the practical range of strain rate suggested by [Pereira and De Gennaro \(2010\)](#),
33
34 378 and (2) fast enough to prevent development of structuration and resistance against loading with
35
36 379 time. The selected strain rates were both too fast to allow fully drained conditions. Excess pore-
37
38 380 water pressure (u_{exc}) was, therefore, built up during the loading stage. Tests were performed in
39
40 381 temperature controlled laboratory environment to avoid the influence of temperature
41
42 382 fluctuations on the output data. In addition to the compression behavior, the water retention
43
44 383 behavior of the test material was also investigated. Table 2 summarizes the details of the CRS
45
46 384 tests. Fig. 7 shows the generalized THM paths followed in the experimental program in a three-
47
48 385 dimensional stress-suction-temperature space.
49
50
51
52
53
54
55
56
57
58
59
60

388

389

Table 2. Details of the CRS tests

Test No.	w_0 [%]	s_0 [kPa]	T [°C]	$\dot{\epsilon}_v$ [s ⁻¹]	σ_p [kPa]
CRSru33-A	33	701	22	4.8×10^{-7}	390
CRSru33-A50	33	701	50	4.8×10^{-7}	295
CRSru33-B	33	701	22	2.4×10^{-6}	480
CRSru32-A	32	802	22	4.8×10^{-7}	490

r: reconstituted, u: unsaturated, A and B: strain rates
The number before dash indicates initial water content.

390

391 *TEST RESULTS*

392 Fig. 8 presents the obtained SWRC (gravimetric water content versus soil suction). The water
 393 retention characteristics of the soil specimen was measured in the new oedometer cell using
 394 axis-translation technique. Moreover, in order to develop a comparison platform, the water
 395 retention curve of an identical specimen was also measured in the new oedometer cell using
 396 the HCTs. Lower water contents were observed at suctions above 600 kPa in the axis-
 397 translation method in comparison with the HCT method. This small difference might be
 398 associated with water evaporation from the top of the sample when using the axis-translation
 399 method. Moreover, the axis-translation method overestimated the AEV of the specimen by
 400 approximately 6% in comparison with the HCT measurements, this deemed to be, in part, due
 401 to the discontinuous data points produced by the axis-translation technique. The new oedometer
 402 cell enables simultaneous and non-destructive measurement of SWRC using both axis-
 403 translation and HCT techniques, along with measurement of specimen's volume change during
 404 the course of drying and wetting. These features allow for more accurate determination of water
 405 retention characteristics (Pasha et al. 2016), in comparison with other methods of SWRC
 406 measurement such as pressure plate.

407 Figs. 9, 10, and 11 present the results of CRS compression tests performed for evaluating the
 408 new oedometer's ability for investigating the coupled effects of strain rate, suction, and

1
2
3 409 temperature. Simplified methods for calculation of unsaturated effective stress can be found in
4
5 410 [Khoshghalb and Khalili \(2013\)](#) and [Khoshghalb et al. \(2015\)](#). However, in this work, the
6
7 411 mechanical path is represented in terms of axial strain (ε_a) and vertical net stress ($\sigma_v - u_a$). Also
8
9 412 shown in the graphs, are the change in pore-water pressure (Δu) with net stress (dotted lines).
10
11 413 For the sake of simplicity, the yield vertical net stress (σ_p) was determined as the intersection
12
13 414 of the best fitted lines to the pseudo-elastic and plastic sections of the compression curve.
14
15
16
17 415 Inspection of suction evolutions recorded by the HCTs revealed that a suction state was
18
19 416 preserved during the compression stages of the carried out experiments, confirming that no
20
21 417 water has been expelled from the unsaturated specimens, and hence, the condition of constant
22
23 418 water content was recognised. The new cell enables continuous monitoring of stress and strain
24
25 419 variations and more accurate estimation of σ_p in comparison with the IL tests. At constant
26
27 420 suction, an increase in σ_p was observed with increase in strain rate (Fig. 9). Similarly, at
28
29 421 constant strain rate, an increase in suction resulted in an increase in σ_p (Fig. 10). Moreover, at
30
31 422 constant suction and strain rate, an increase in temperature resulted in a decrease in σ_p (Fig.
32
33 423 11). Similar results have been reported in the literature. For instance, [François et al. \(2007\)](#) and
34
35 424 [Salager et al. \(2008\)](#) performed a set of temperature controlled oedometer tests on unsaturated
36
37 425 sandy silt material from the region of Sion in Switzerland, and reported an increase in σ_p with
38
39 426 increase in suction, and a decrease in σ_p with increase in temperature. [Pereira and De Gennaro](#)
40
41 427 [\(2010\)](#) performed isotropic compression tests on unsaturated chalk material at various strain
42
43 428 rates and reported an increase in σ_p with increase in strain rate. Similar results (i.e. increase in
44
45 429 σ_p with suction and decrease in σ_p with temperature) were reported by [Uchaipichat and Khalili](#)
46
47 430 [\(2009\)](#) from a set of suction and temperature controlled isotropic tests on a laboratory-
48
49 431 compacted silt from the Bourke region of New South Wales, Australia.
50
51
52
53
54
55
56
57
58
59
60

1
2
3 432 In order to investigate the effect of temperature on HCT measurements during an experiment,
4
5 433 a soil specimen was subjected to a heating/cooling cycle of 25 to 65° C in steps of 10° C (Fig.
6
7 434 12). For each stage of heating, a sudden increase in u_w (decrease in suction) followed by
8
9 435 dissipation of the developed u_{exc} was observed. Similarly, for each stage of cooling, a decrease
10
11 436 in u_w (increase in suction) followed by a return of measurements to their initial values was
12
13 437 observed. Overall, throughout the course of heating and cooling, a small increase in soil suction
14
15 438 was observed. The reason behind the observed increase in soil suction is unknown. The heating
16
17 439 cycle may change the structural properties of the localized unsaturated pockets in the specimen
18
19 440 in vicinity of the HCTs and hence affect the suction measurements. These possible changes
20
21 441 may not be fully recovered during the cooling cycle resulting in less evident suction changes
22
23 442 during cooling steps. Fig. 13 shows the axial deformation of the specimen during heating and
24
25 443 cooling cycles. The vertical displacements were corrected, for the effect of cell structure
26
27 444 dilation, based on the Equation 1. Development and the subsequent dissipation of the u_{exc}
28
29 445 during stepwise heating resulted in development of volumetric strain in the specimen as shown
30
31 446 in Fig. 14.
32
33
34
35
36
37
38
39

40 447 Conclusions

41
42 448 Climatic variations results in development of non-isothermal and unsaturated conditions in soil
43
44 449 deposits, arising the need for advanced experimental characterization of soils' mechanical
45
46 450 response taking into account the coupled effects of temperature, suction, and loading rate. The
47
48 451 specific features of the newly designed cell enables precise investigation of the THM properties
49
50 452 of soils over suction, temperature, and strain rate ranges of practical interest. The distinct
51
52 453 features of the new cell are
53
54
55
56
57
58
59
60

- 1
2
3 454 - Incorporation of two suction measurement/control techniques, i.e. axis-translation and
4
5 455 HCT, for enhanced and accurate monitoring of suction evolutions especially in long-
6
7 term tests.
8 456
9
10 457 - Enlarged specimen size to capture the macrostructural effects on the THM response of
11
12 458 natural clays.
13
14 459 - Broad temperature measurement range of up to 200° C.
15
16
17 460 - Significant reduction in the equilibrium time by using a tubular heating element at the
18
19 461 base of the cell to overcome the delays associated with thermal conductivity of the
20
21 462 metallic cell body.
22
23
24

25 463 The reliability of the experimental results is a function of adequate calibration of the testing
26
27 464 system. The new cell was rigorously calibrated to account for the delay in thermal equilibrium
28
29 465 between the heating system and the specimen, and the effect of temperature on cell structure
30
31 466 deformation and the response of HCTs. The calibration coefficient of the HCT was found to
32
33 467 be unaffected by change in temperature. The paper also presents useful information on
34
35 468 necessary corrections to be applied to the measured data using THM cells.
36
37
38
39

40 469 The preliminary results of SWRC measurement and CRS compression tests with this apparatus
41
42 470 are promising for its application in soil mechanics laboratories. The results of constant water
43
44 471 content tests where temperature, suction, and strain rate were modified, have been presented.
45
46 472 It was shown that the cell is capable of measuring and observing the changing trends in the
47
48 473 preconsolidation stress with temperature, strain rate, and suction.
49
50
51
52

53 474 Acknowledgments

54
55
56 475 The authors are grateful to Mr Graeme Thacker of the engineering workshop at the University
57
58 476 of Warwick for his useful suggestions in design and manufacturing the apparatus presented.
59
60

1
2
3 477 References
4

- 5
6 478 ASTM-D4186-06, 2006, *Standard Test Method for One-dimensional Consolidation Properties*
7
8 479 *of Saturated Cohesive Soils Using Controlled-strain Loading*, ASTM International,
9
10 480 West Conshohoken, PA, www.astm.org.
11
12
13 481 Bagheri, M., Rezania, M. and Mousavi Nezhad, M., “An Experimental Study of the Initial
14
15 482 Volumetric Strain Rate Effect on the Creep Behaviour of Reconstituted Clays,” In IOP
16
17 483 Conference Series: Earth and Environmental Science, Vol. 26, No. 1, 2015, IOP
18
19 484 Publishing, p. 012034.
20
21
22 485 Bagheri, M., Rezania, M. and Mousavi Nezhad, M., “Cavitation in High-Capacity
23
24 486 Tensiometers: Effect of Water Reservoir Surface Roughness,” *Geotech. Research.*,
25
26 487 Vol. 5, No.2, 2018, pp. 81-95, <https://doi.org/10.1680/jgere.17.00016>.
27
28
29 488 Burghignoli, A., Desideri, A. and Miliziano, S., “A Laboratory Study on Thermomechanical
30
31 489 Behaviour of Clayey Soils,” *Can. Geotech. J.*, Vol. 37, No. 4, 2000, pp. 764-780,
32
33 490 <https://doi.org/10.1139/t00-010>.
34
35
36 491 Cekerevac, C. and Laloui, L., “Experimental Study of Thermal Effects on the Mechanical
37
38 492 Behaviour of a Clay,” *Int. J. Numer. Anal. Methods Geomech*, Vol. 28, No. 3, 2004,
39
40 493 pp. 209-228, <https://doi.org/10.1002/nag.332>.
41
42
43 494 Coccia, C.J.R. and McCartney, J.S., “Thermal Volume Change of Poorly Draining Soils I:
44
45 495 Critical Assessment of Volume Change Mechanisms.” *Comp. Geotech.*, Vol. 80
46
47 496 (December), 2016, pp. 26-40. <https://doi.org/10.1016/j.compgeo.2016.06.009>.
48
49
50 497 Craig, R. F., 2004, *Craig's Soil Mechanics*, Spon Press, London, p. 552.
51
52 498 Delage, P., Sultan, N. and Cui, Y.J., “On the Thermal Consolidation of Boom Clay,” *Can*
53
54 499 *Geotech. J.*, Vol. 37, No. 2, 2000, pp. 343-354, <https://doi.org/10.1139/t99-105>.
55
56
57
58
59
60

- 1
2
3 500 Fodil, A., Aloulou, W. and Hicher, P. Y., “Viscoplastic Behaviour of Soft Clay,”
4
5 501 *Géotechnique*, Vol. 47, No. 3, 1997, pp. 581-591,
6
7 <https://doi.org/10.1680/geot.1997.47.3.581>.
8 502
9
10 503 François, B. and Laloui, L., “An Oedometer for Studying Combined Effects of Temperature
11
12 504 and Suction on Soils,” *Geotech. Test. J.*, Vol. 33, No. 2, 2010, pp. 112-122,
13
14 <https://doi.org/10.1520/GTJ102348>.
15 505
16
17 506 François, B., Salager, S., El Youssoufi, M.S., Ubals Picanyol, D., Laloui, L. and Saix, C.,
18
19 507 “Compression Tests on a Sandy Silt at Different Suction and Temperature Levels,”
20
21 508 *Comp. Appl. Geotech. Eng.*, GSP 157, ASCE, 2007, pp. 1-10,
22
23 doi:10.1061/40901(220)11.
24 509
25
26 510 Garga, V.K., “Effect of Sample Size on Consolidation of a Fissured Clay”. *Can. Geotech. J.*,
27
28 511 Vol. 25, No. 1, 1988, pp. 76-84, <https://doi.org/10.1139/t88-009>.
29
30
31 512 Gasparre, A., 2005, *Advanced laboratory characterisation of London Clay*. Ph.D. Thesis,
32
33 513 University of London.
34
35 514 Jarad, N., Cuisinier, O. and Masrouri, F., “Effect of Temperature and Strain Rate on the
36
37 515 Consolidation Behaviour of Compacted Clayey Soils,” *Europ. J. Environ. Civil Eng.*,
38
39 Vol. 21, 2017, pp. 1-18, <https://doi.org/10.1080/19648189.2017.1311806>.
40 516
41
42 517 Khoshghalb, A. and Khalili, N. “A Meshfree Method for Fully Coupled Analysis of Flow and
43
44 518 Deformation in Unsaturated Porous Media.” *Int. J. Numeric. Anal. Methods Geomech.*,
45
46 519 2013, Vol. 37, No. 7, pp. 716-743, <https://doi.org/10.1002/nag.1120>.
47
48
49 520 Khoshghalb, A., Pasha, A. Y. and Khalili, N., “A Fractal Model for Volume Change
50
51 521 Dependency of the Water Retention Curve.” *Géotechnique*, 2015, Vol. 62, No. 2, pp.
52
53 522 141-146, <https://doi.org/10.1680/geot.14.T.016>.
54
55
56 523 Lai, X., Wang, S., Qin, H. and Liu, X., “Unsaturated Creep Tests and Empirical Models for
57
58 524 Sliding Zone Soils of Qianjiangping Landslide in the Three Gorges,” *J. Rock Mech.*
59
60

- 1
2
3 525 *Geotech. Eng.*, Vol.2, No. 2, 2010, pp. 149-154,
4
5
6 526 <https://doi.org/10.3724/SP.J.1235.2010.00149>.
7
8 527 Le, T. M., Fatahi, B. and Khabbaz, H., “Viscous Behavior of Soft Clay and Inducing Factor”,
9
10 528 *Geotech. Geolog. Eng.*, Vol. 30, 2012, pp. 1069-1083, [https://doi.org/10.1007/s10706-](https://doi.org/10.1007/s10706-012-9535-0)
11
12 529 [012-9535-0](https://doi.org/10.1007/s10706-012-9535-0).
13
14
15 530 Marinho, F.A.M., Take, W.A. and Tarantino, A., “Measurement of Matric Suction Using
16
17 531 Tensiometric and Axis Translation Techniques,” *Geotech. Geolog. Eng.*, Vol. 26, No.
18
19 532 6, 2008, pp. 615-631, <http://dx.doi.org/10.1007/s10706-008-9201-8>.
20
21
22 533 Muñoz-castelblanco, J., Delage, P., Pereira, J. M. and Cui, Y.J., “Some Aspects of the
23
24 534 Compression and Collapse Behaviour of an Unsaturated Natural Loess,” *Géotechnique*
25
26 535 *Letters*, Vol. 1, No. 2, 2011, pp. 17-22, <https://doi.org/10.1680/geolett.11.00003>.
27
28
29 536 Ng, C.W.W. and Xu, J., “Effects of Current Suction Ratio and Recent Suction History on
30
31 537 Small-Strain Behaviour of an Unsaturated Soil,” *Can. Geotech. J.*, Vol. 49, No. 2, 2012,
32
33 538 pp. 226-243, <https://doi.org/10.1139/t11-097>.
34
35
36 539 Ng, C.W.W, Mu, Q.Y., and Zhou, C., “Effects of Boundary Conditions on Cyclic Thermal
37
38 540 Strains of Clay and Sand”, *Geotech. Letters*, Vol. 7, No. 1, 2017, pp. 1-6,
39
40 541 <https://doi.org/10.1680/jgele.16.00155>.
41
42
43 542 Pagano, A. Tarantino, A., Bagheri, M., Rezanian, M. and Sentenac, Ph., “An Experimental
44
45 543 Investigation of the Independent Effect of Suction and Degree of Saturation on Very
46
47 544 Small-Strain Stiffness of Unsaturated Sand,” presented at the Third European
48
49 545 Conference on Unsaturated Soils, E-UNSAT2016, September 12–14, 2016, E3S Web
50
51 546 of Conferences, Vol. 9, p. 4, <https://doi.org/10.1051/e3sconf/20160914015>.
52
53
54 547 Pasha A. Y., Khoshghalb, A. and Khalili, N., “Pitfalls in Interpretation of Gravimetric Water
55
56 548 Content–Based Soil-Water Characteristic Curve for Deformable Porous Media” *Int. J.*

- 1
2
3 549 *Geomech.*, 2016, Vol. 16, No. 6, D4015004, [https://doi.org/10.1061/\(ASCE\)GM.1943-](https://doi.org/10.1061/(ASCE)GM.1943-)
4
5 550 [5622.0000570](https://doi.org/10.1061/(ASCE)GM.1943-5622.0000570).
6
7
8 551 Pereira, J.M. and De Gennaro, V., “On the Time-Dependent Behaviour of Unsaturated
9
10 552 Geomaterials,” presented at the Fifth International Conference on Unsaturated Soils,
11
12 553 Barcelona, Spain, September 6–8, 2010, CRC Press, pp. 921-925.
13
14
15 554 Rampino, C., Mancuso, C. and Vinale, F., “Laboratory Testing on an Unsaturated Soil:
16
17 555 Equipment, Procedures, and First Experimental Results,” *Can. Geotech. J.*, Vol. 36,
18
19 556 No. 1, 1999, pp. 1-12, <https://doi.org/10.1139/t98-093>.
20
21
22 557 Rezania, M., Bagheri, M., Mousavi Nezhad, M. and Sivasithamparam, N., “Creep Analysis of
23
24 558 an Earth Embankment on Soft Soil deposit with and without PVD Improvement,”
25
26 559 *Geotext. Geomemb.*, Vol. 45, No. 5, 2017, pp. 537-547,
27
28 560 <https://doi.org/10.1016/j.geotexmem.2017.07.004>.
29
30
31 561 Rezania, M., Mousavi Nezhad, M., Zanganeh, H., Castro, J. and Sivasithamparam, N.,
32
33 562 “Modeling Pile Setup in Natural Clay Deposit Considering Soil Anisotropy, Structure,
34
35 563 and Creep Effects: Case Study.” *Int. J. Geomech.* Vol. 17, No. 3, 2016, p. 04016075.
36
37 564 [https://doi.org/10.1061/\(ASCE\)GM.1943-5622.0000774](https://doi.org/10.1061/(ASCE)GM.1943-5622.0000774).
38
39
40 565 Romero, E., Gens, A. and Lloret, A., “Suction Effects on a Compacted Clay under Non-
41
42 566 Isothermal Conditions,” *Géotechnique*, Vol. 53, No. 1, 2003, pp. 65-81,
43
44 567 <https://doi.org/10.1680/geot.2003.53.1.65>.
45
46
47 568 Romero, E., Lloret, A. and Gens, A., “Development of a New Suction and Temperature
48
49 569 Controlled Oedometer Cell,” presented at the First International Conference on
50
51 570 Unsaturated Soils, Paris, September 6–8, 1995, A.A. Balkema/Presses des Ponts et
52
53 571 Chaussees, pp. 553-559.
54
55
56
57
58
59
60

- 1
2
3 572 Romero, E., Villar, M.V. and Lloret, A., “Thermo-Hydro-Mechanical Behavior of Two
4
5 573 Heavily Overconsolidated Clays,” *Eng. Geology J.*, Vol. 81, No. 3, 2005, pp. 255-268,
6
7
8 574 <https://doi.org/10.1016/j.enggeo.2005.06.011>.
- 9
10 575 Rowe, P.W. and Barden, L., “A New Consolidation Cell,” *Géotechnique*, Vol. 16, No. 2, 1966,
11
12 576 pp. 162-170, <https://doi.org/10.1680/geot.1966.16.2.162>.
- 13
14 577 Salager, S., François, B., El Yousoufi, M.S., Laloui, L. and Saix, C., “Experimental
15
16 578 Investigations on Temperature and Suction Effects on Compressibility and Pre-
17
18 579 Consolidation Pressure of a Sandy Silt,” *Soils Found.*, Vol. 48, No. 4, 2008, pp. 453–
19
20 580 466, <https://doi.org/10.3208/sandf.48.453>.
- 21
22 581 Sample, K.M. and Shakelford, C.D. “Apparatus for Constant Rate-of-Strain Consolidation of
23
24 582 Slurry Mixed Soils,” *Geotech. Test. J.*, Vol. 35, No. 3, 2012, pp. 409-419,
25
26 583 <https://doi.org/10.1520/GTJ103787>.
- 27
28 584 Seah, T.H. and Juirnarongrit, T., “Constant Rate of Strain Consolidation with Radial
29
30 585 Drainage,” *Geotech. Test. J.*, Vol. 26, No. 4, 2003, pp. 432-443,
31
32 586 <https://doi.org/10.1520/GTJ11251J>.
- 33
34 587 Tarantino, A. and De Col, E., “Compaction Behavior of Clay,” *Géotechnique*, Vol. 58, No. 3,
35
36 588 2008, pp. 199-213, <https://doi.org/10.1680/geot.2008.58.3.199>.
- 37
38 589 Tsutsumi, A. and Tanaka, H. “Compressive Behavior During the Transition of Strain Rate,”
39
40 590 *Soils Found.*, Vol. 51, No. 5, 2011, pp. 813-822, <https://doi.org/10.3208/sandf.51.813>.
- 41
42 591 Uchaipichat, A. and Khalili, N., “Experimental Investigation of Thermo-Hydro-Mechanical
43
44 592 Behaviour of an Unsaturated Silt,” *Géotechnique*, Vol. 59, No. 4, 2009, pp. 339-353,
45
46 593 <https://doi.org/10.1680/geot.2009.59.4.339>.
- 47
48 594 Wissa, A.E.Z. and Heiberg, S., “A New One-Dimensional Consolidation Test,” Department of
49
50 595 Civil Engineering Research Report 69-9, Soil Publication, No. 229, Massachusetts
51
52 596 Institute of Technology, Cambridge, MA, 1969.
- 53
54
55
56
57
58
59
60

1
2
3 597 Zou, L., Wang, S. and Lai, X., “Creep Model for Unsaturated Soils in Sliding Zone of
4
5 598 Qianjiangping Landslide,” *J. Rock Mech. Geotech. Eng.*, Vol. 5, No. 2, 2013, pp. 162-
6
7 599 167, <https://doi.org/10.1016/j.jrmge.2013.03.001>.
8
9

10 600
11
12
13
14
15
16
17
18
19
20
21
22
23
24
25
26
27
28
29
30
31
32
33
34
35
36
37
38
39
40
41
42
43
44
45
46
47
48
49
50
51
52
53
54
55
56
57
58
59
60

For Review Only

1
2
3 601 Figure Captions
4
5

6 602 Fig. 1 Schematic diagram of the CRS cell structure and components
7

8 603 Fig. 2 The CRS system layout
9

10 604 Fig. 3 Effect of thermal expansion of the cell on the measured axial deformations
11

12 605 Fig. 4 Saturation chamber: (a) schematic diagram; (b) photo
13
14

15 606 Fig. 5 Effect of temperature on HCT calibration
16
17

18 607 Fig. 6 Time lag in temperature equilibrium between the heating system and the soil specimen
19

20 608 Fig. 7 Generalized THM paths followed in the experimental program. Paths A and B:
21 isothermal compression with suction and strain rate control (CRSru33-A, CRSru33-B, and
22 CRSru32-A); Path C: non-isothermal compression with suction and strain rate control
23 (CRSru33-A50)
24
25
26
27

28 609 Fig. 8 SWRC determined for main drying path
29

30 610 Fig. 9 Effect of strain rate on compression response at constant suction
31
32

33 611 Fig. 10 Effect of suction on compression response at constant strain rate
34
35

36 612 Fig. 11 Effect of temperature on compression response at constant suction and strain rate
37
38

39 613 Fig. 12 Effect of temperature on HCT measurement
40
41

42 614 Fig. 13 Vertical displacement of the soil specimen during heating and cooling cycles
43
44

45 615 Fig. 14 Thermally induced volumetric strain during heating and cooling cycles
46
47
48
49
50
51
52
53
54
55
56
57
58
59
60

1
2
3
4
5
6
7
8
9
10
11
12
13
14
15
16
17
18
19
20
21
22
23
24
25
26
27
28
29
30
31
32
33
34
35
36
37
38
39
40
41
42
43
44
45
46
47
48
49
50
51
52
53
54
55
56
57
58
59
60

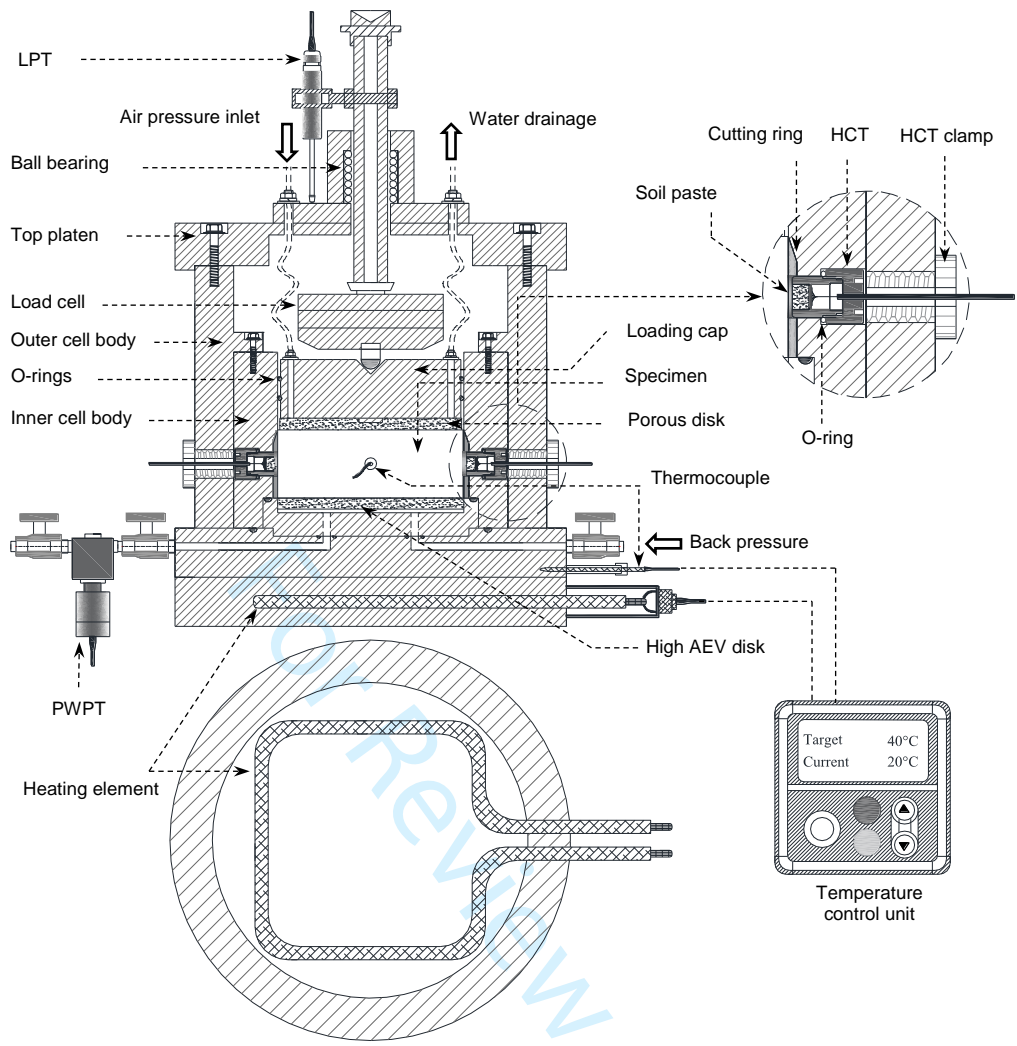


Fig. 1 Schematic diagram of the CRS cell structure and components

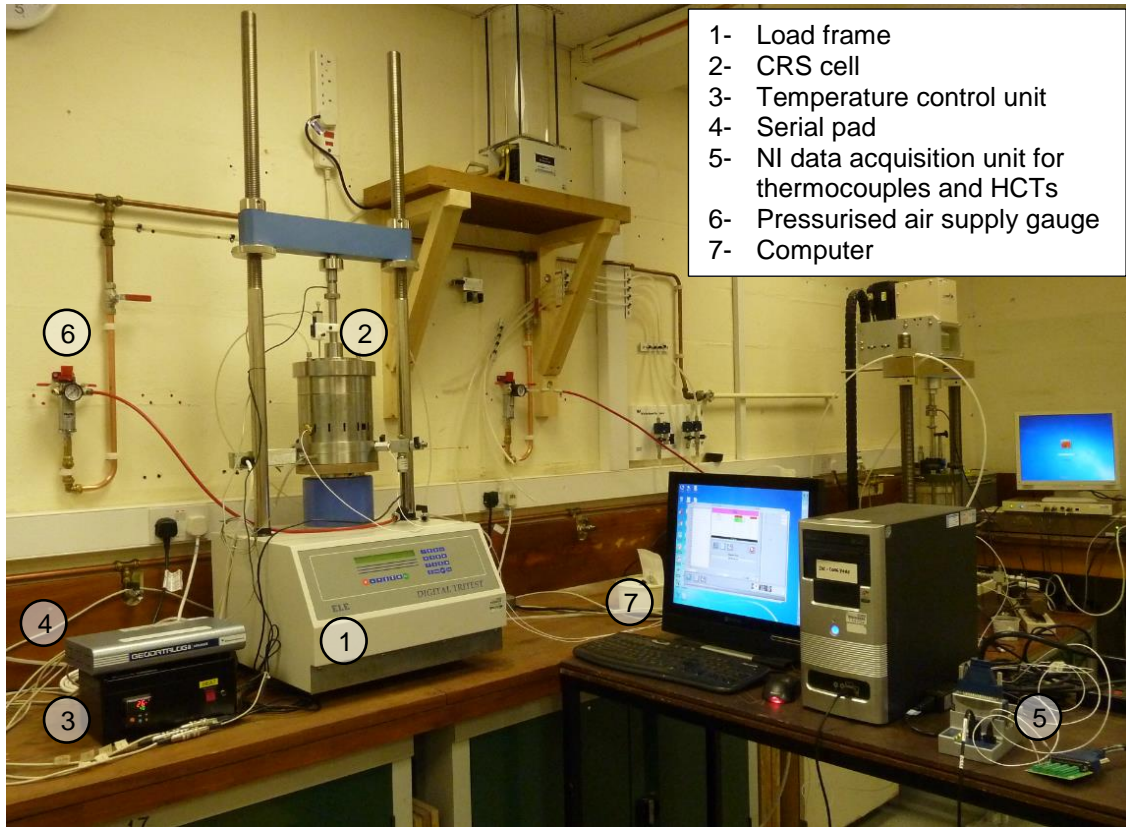


Fig. 2 The CRS system layout

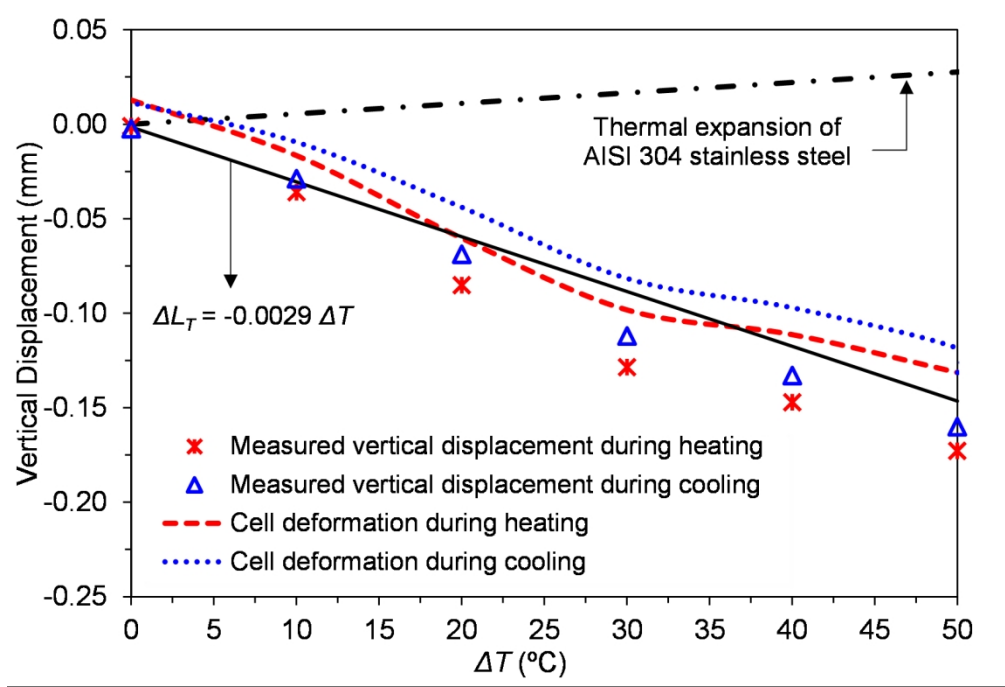


Fig. 3 Effect of thermal expansion of the cell on the measured axial deformations
150x103mm (300 x 300 DPI)

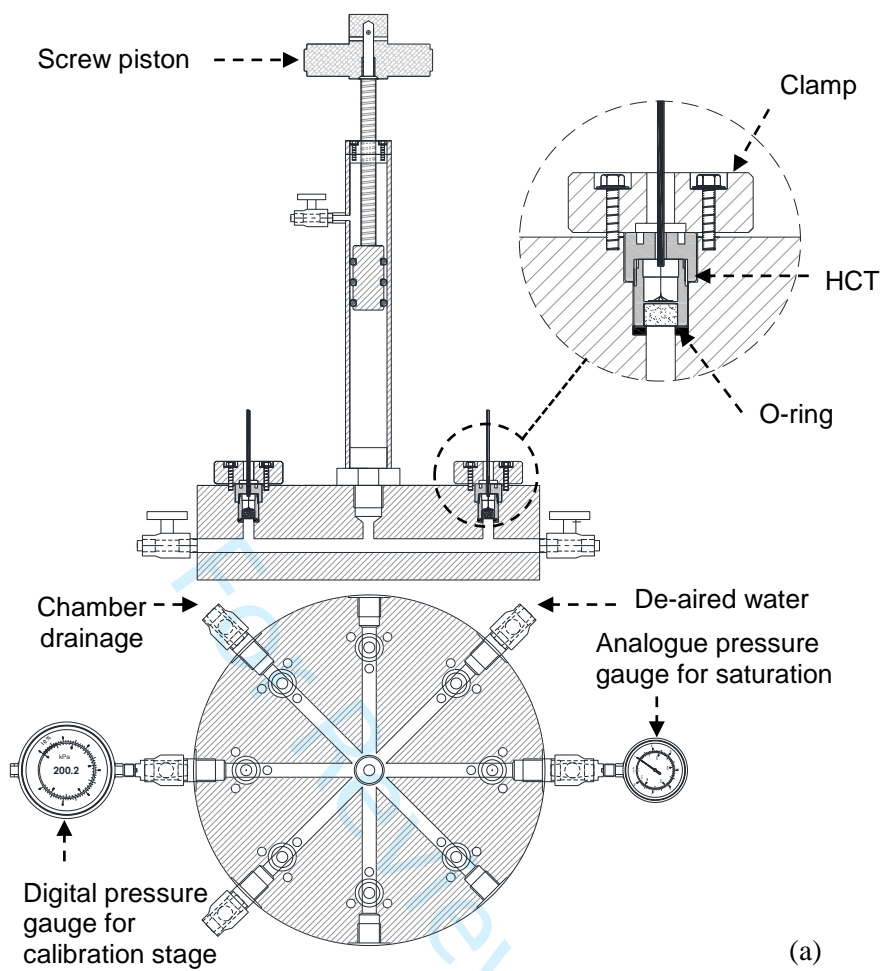


Fig. 4 Saturation chamber: (a) schematic diagram; (b) photo

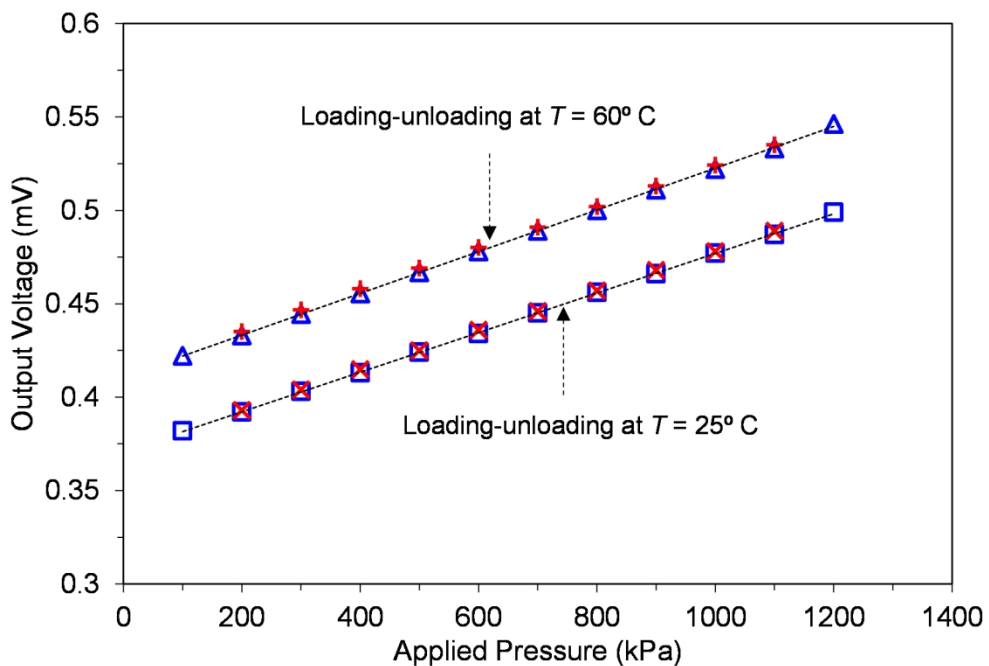


Fig. 5 Effect of temperature on HCT calibration
150x103mm (300 x 300 DPI)

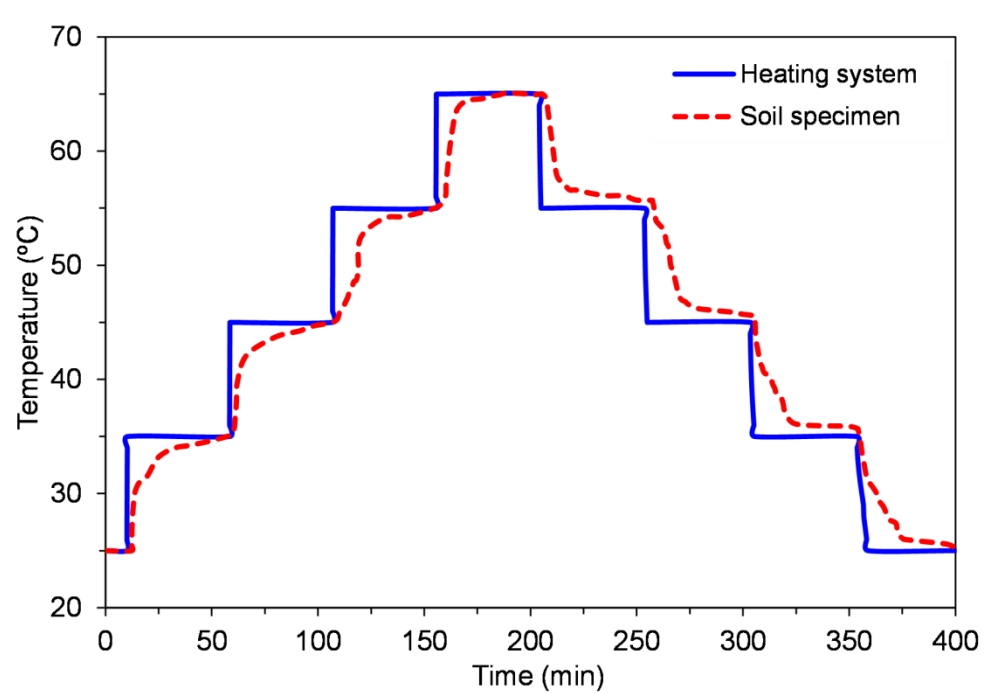


Fig. 6 Time lag in temperature equilibrium between the heating system and the soil specimen

150x103mm (300 x 300 DPI)

1
2
3
4
5
6
7
8
9
10
11
12
13
14
15
16
17
18
19
20
21
22
23
24
25
26
27
28
29
30
31
32
33
34
35
36
37
38
39
40
41
42
43
44
45
46
47
48
49
50
51
52
53
54
55
56
57
58
59
60

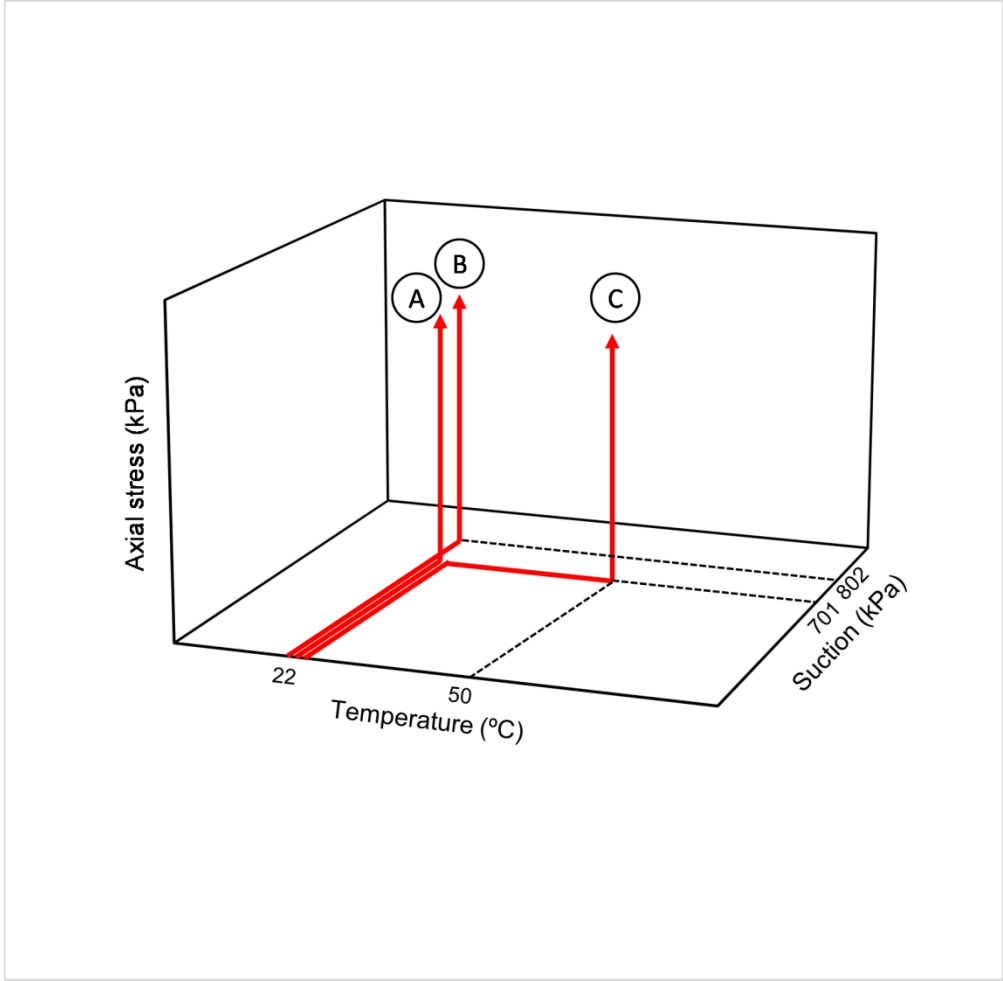


Fig. 7 Generalized THM paths followed in the experimental program. Paths A and B: isothermal compression with suction and strain rate control (CRSru33-A, CRSru33-B, and CRSru32-A); Path C: non-isothermal compression with suction and strain rate control (CRSru33-A50)

147x144mm (300 x 300 DPI)

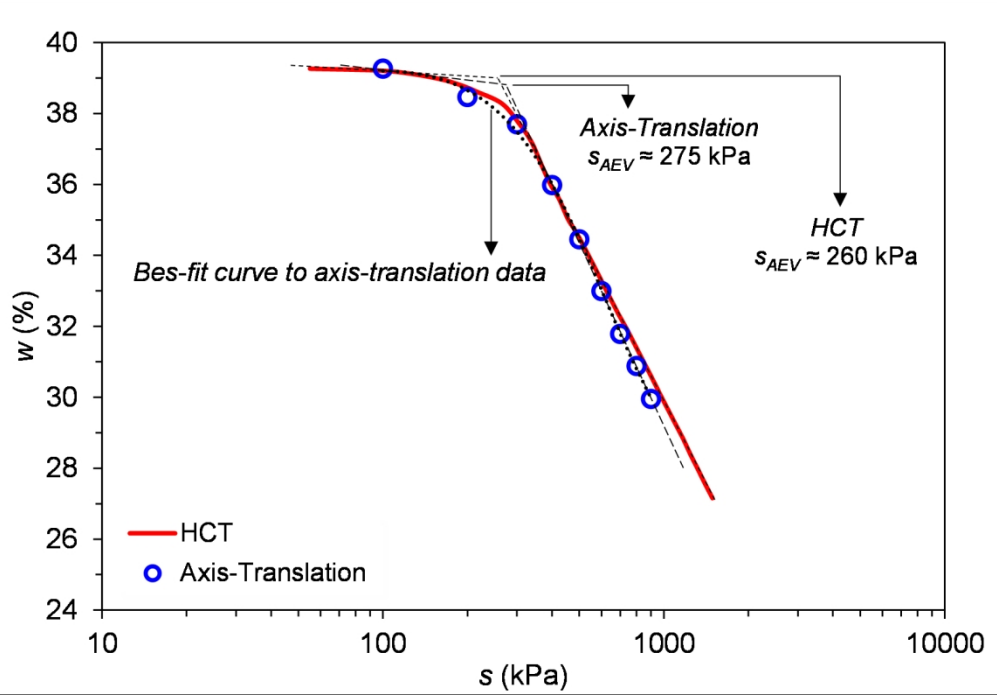


Fig. 8 SWRC determined for main drying path
 149x103mm (300 x 300 DPI)

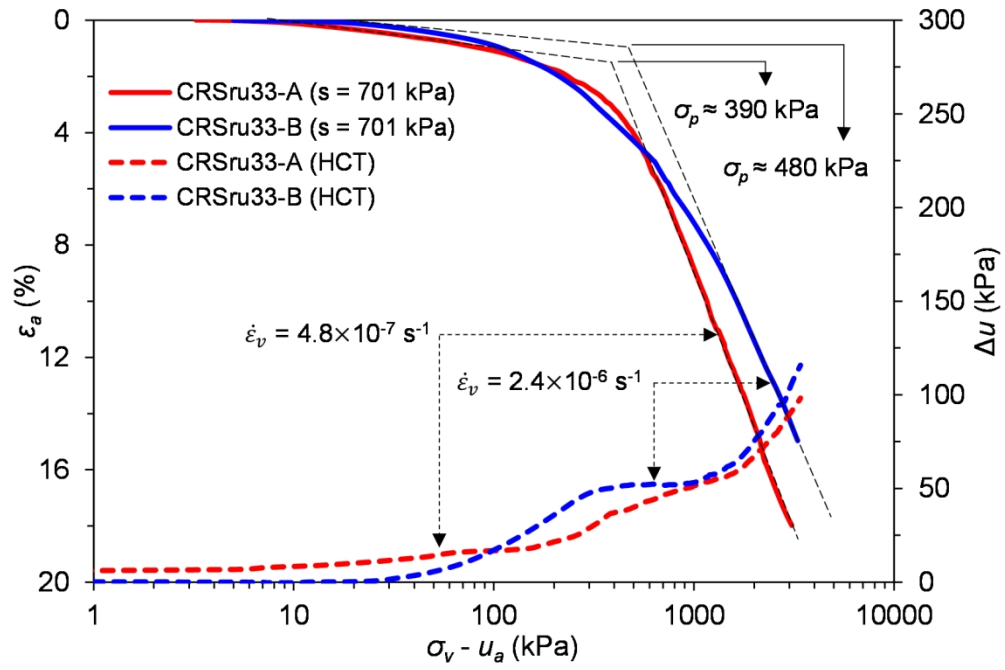


Fig. 9 Effect of strain rate on compression response at constant suction
150x103mm (300 x 300 DPI)

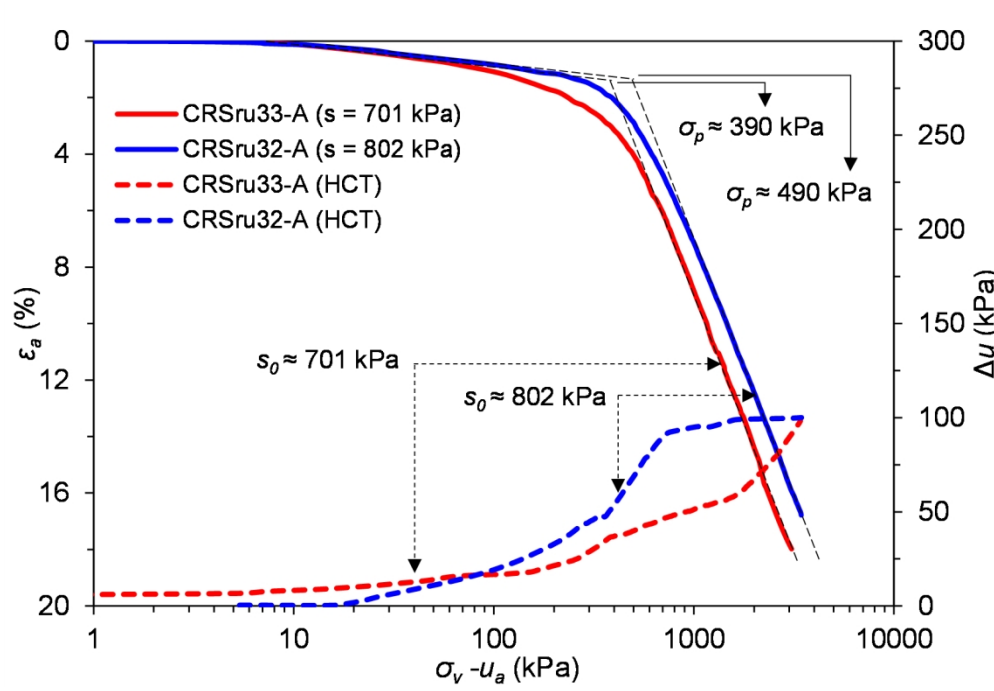


Fig. 10 Effect of suction on compression response at constant strain rate
150x103mm (300 x 300 DPI)

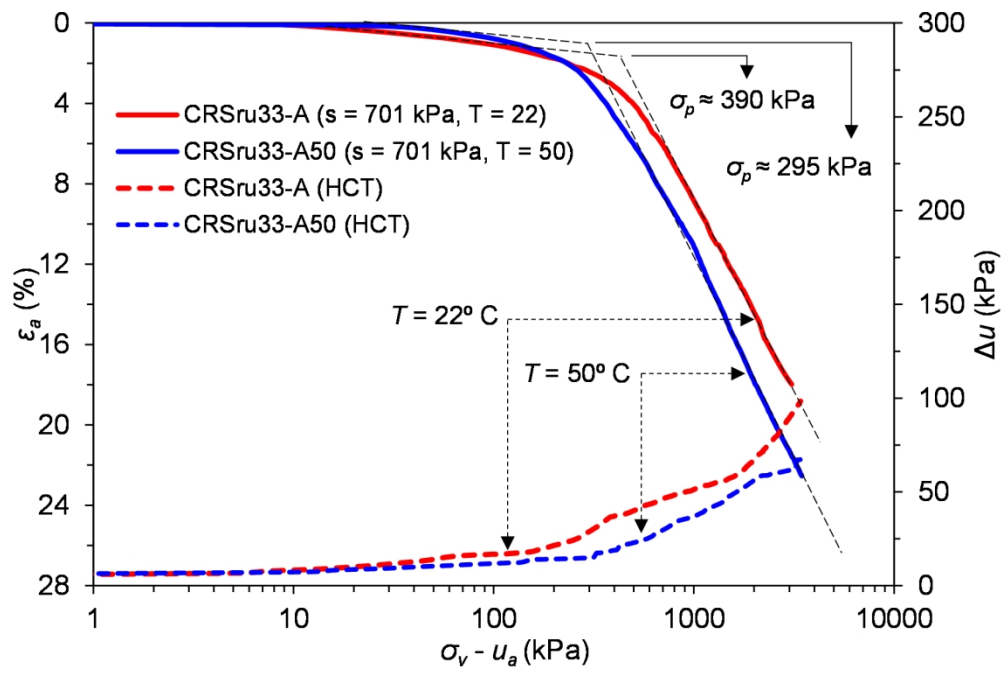


Fig. 11 Effect of temperature on compression response at constant suction and strain rate
150x103mm (300 x 300 DPI)

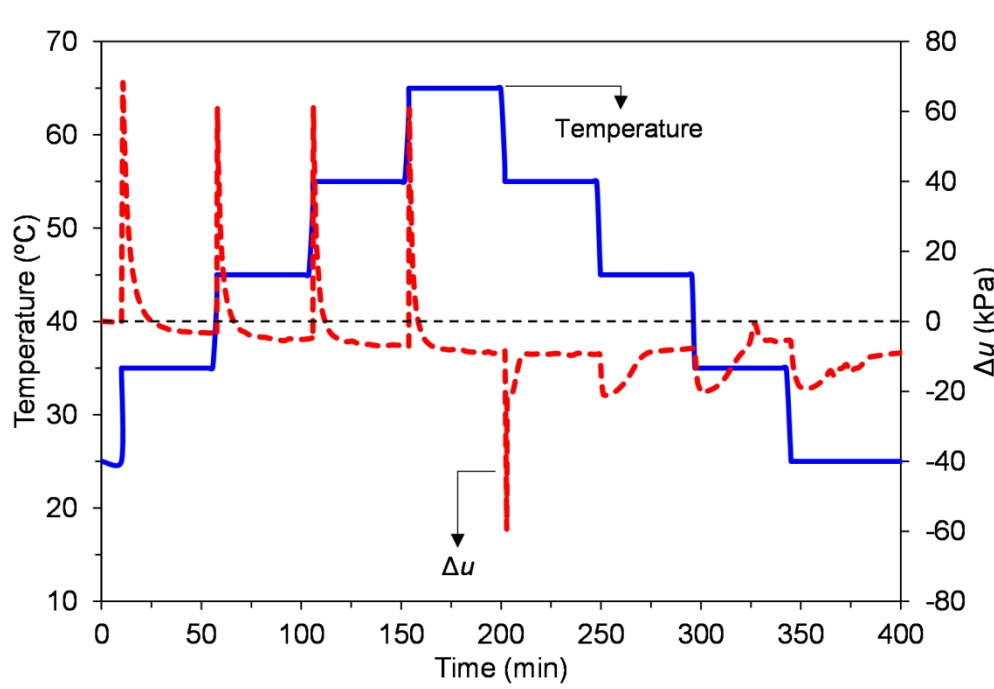


Fig. 12 Effect of temperature on HCT measurement

150x103mm (300 x 300 DPI)

1
2
3
4
5
6
7
8
9
10
11
12
13
14
15
16
17
18
19
20
21
22
23
24
25
26
27
28
29
30
31
32
33
34
35
36
37
38
39
40
41
42
43
44
45
46
47
48
49
50
51
52
53
54
55
56
57
58
59
60

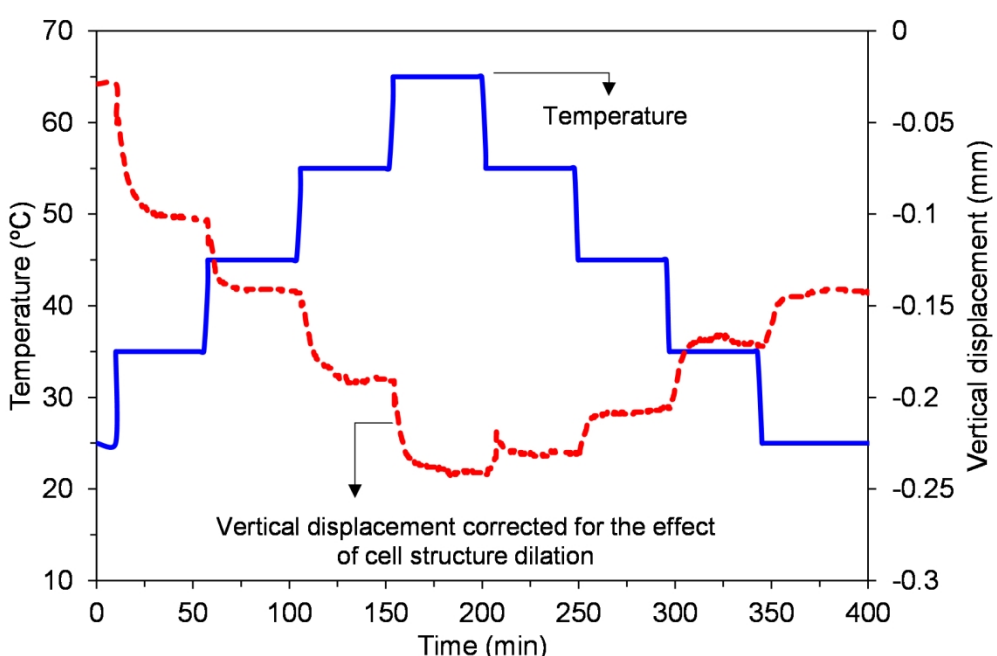


Fig. 13 Vertical displacement of the soil specimen during heating and cooling cycles
154x103mm (300 x 300 DPI)

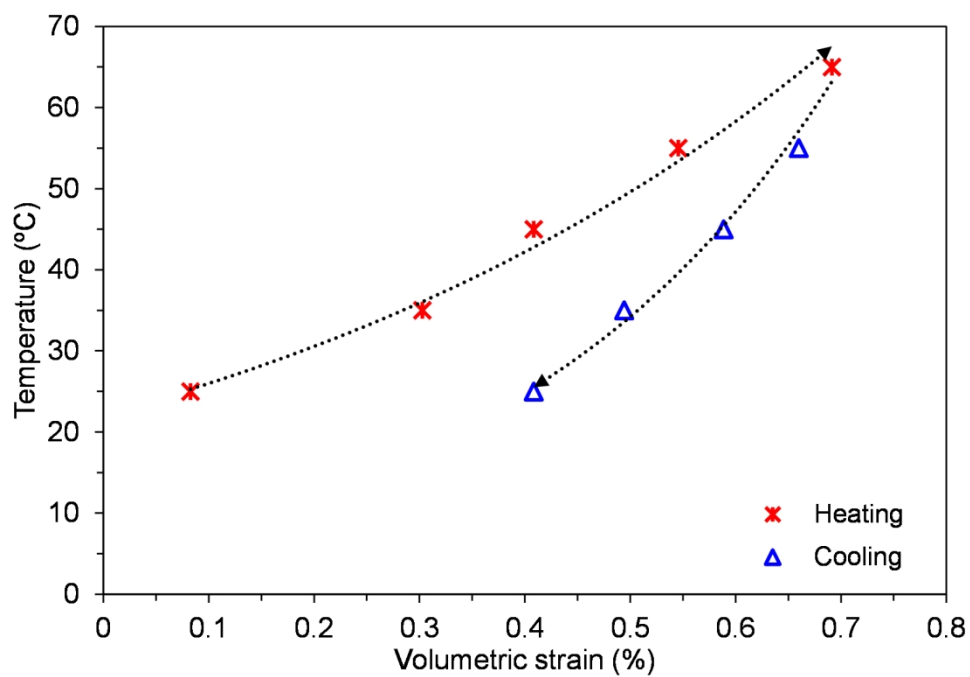


Fig. 14 Thermally induced volumetric strain during heating and cooling cycles

149x103mm (300 x 300 DPI)